UDK 661.847'02:544.526.5
Original scientific article/Izvirni znanstveni članek

ISSN 1580-2949
Mater. Tehnol.

SYNTHESIS OF MORPHOLOGY-CONTROLLED ZnO NANOSTRUCTURES AND EVALUATION OF THEIR PHOTOCATALYTIC AND GAS-SENSING PROPERTIES

SINTEZA MORFOLOGIJE KONTROLIRANIH ZnO NANOSTRUKTUR IN OVREDNOTENJE NJIHOVIH FOTOKATALITIČNIH IN PLINSKO-SENZORSKIH LASTNOSTI

Shu Cui[1,2], Haixin Zhao[2], Chengyou Liu[3], Hai Yu[1], Nan Li[2], Xiaotian Li[2]*

[1]School of Physics, Tonghua Normal University, Tonghua, Jilin 134002, China
[2]College of Material Science and Engineering, Key Laboratory of Automobile Materials of Ministry of Education, Jilin University, 2699 Qianjin Street, Changchun 130012, China
[3]School of Chemistry and Materials Engineering, Hainan Vocational University of Science and Technology, Hainan 570000, China

Prejem rokopisa – received: 2025-03-20; sprejem za objavo – accepted for publication: 2025-08-18

doi:10.17222/mit.2025.1424

ZnO samples with two distinct morphologies (porous particles and grenade-like structures) were synthesized via a sol-gel-hydrothermal method in a water-ethylene glycol binary solvent. By tuning the zinc precursor concentration, the morphologies were precisely controlled. In the investigation of photocatalytic properties, we evaluated the material's ability to degrade the organic dye Rhodamine B (RB) under UV light. Additionally, we analyzed the active radicals generated during photocatalysis and evaluated the material's recyclability. In the study of gas-sensing properties, we conducted a series of performance tests under various conditions, including temperature, gas concentration, cycle stability, response and recovery times, and comparative responses in different atmospheres. Our results showed that the samples exhibited superior ethanol selectivity. Moreover, all samples exhibited excellent cycle stability and fast response times. The small size and porous structure of the samples significantly enhanced their gas-sensing performance by providing ample channels and space for gas diffusion and reaction during testing. This unique morphology significantly improved the material's gas-sensing performance.

Keywords: zinc oxide, synthesis, photocatalysis, gas sensing, ethanol

Avtorji članka so s sol-gel-hidrotermalno metodo v binarni etilen glikolni vodni raztopini sintetizirali vzorce nano delcev ZnO. Delci so imeli dve izraziti morfologiji; prvi so bili porozni sferični delci in drugi delci v obliki nano "granatk". Z uglaševanjem koncentracije prekurzorja cinka so natančno kontrolirali morfologijo Zno nano delcev. Nato so ugotavljali njihove fotokatalitične lastnosti in ocenili njihovo sposobnost za degradacijo organske barve Rhodamine B (RB) pod ultra vijolično (UV) svetlobo. Dodatno so avtorji analizirali še aktivne radikale, ki so se generirali med fotokatalizo in ocenili sposobnost materiala za recikliranje. Študij lastnosti pomembnih za plinske senzorje so avtorji določali pri različnih pogojih, vključno z vplivom temperature, koncentracije plina, stabilnosti ciklusa, odzivnega in obnovitvenega časa ter primerjave odziva v različnih atmosferah. Rezultati raziskav so pokazali, da imajo sintetizirani vzorci vrhunsko selektivnost etanola. Nadalje so imeli vsi vzorci odlično stabilnost ciklusa in hiter odzivni čas. Majhna velikost delcev in njihova porozna struktura pomembno izboljšujeta njihove plinske senzorske lastnosti z zagotavljanjem dovolj velikega števila kanalčkov za difuzijo plina med testiranjem. Ta unikatna morfologija delcev ZnO pomembno izboljšuje plinske senzorske lastnosti tega materiala.

Ključne besede: cinkov oksid, nano delci, sinteza, fotokataliza, plinski senzorji, etanol

1 INTRODUCTION

Industrialization and urbanization have intensified environmental pollution, particularly water and air contamination. Photocatalysis and gas-sensing technologies are considered promising solutions for pollutant degradation and trace gas detection, respectively.

Zinc oxide (ZnO), a typical n-type semiconductor metal oxide, exhibits exceptional physical and chemical properties, underscoring its vast application potential across multiple domains. In photocatalysis, ZnO is comparable to titanium dioxide (TiO_2), renowned for its physicochemical stability, non-toxicity, cost-effectiveness, and high photocatalytic efficiency.[1–7] These attributes position ZnO as a preferred material for organic pollutant remediation in aqueous environments. Additionally, ZnO is a pivotal gas-sensitive material in gas sensor research, demonstrating significant sensitivity to various gases, including ethanol,[8] nitrogen dioxide,[9] acetone,[9] and hydrogen.[10]

The composition, size, and morphology of a material are key factors influencing its properties, guiding current ZnO research in three main directions: elemental doping (e.g., Au,[10] Pt,[10,11] Ag[12]), integration with heterogeneous semiconductors (e.g., CuO,[13] C_3N_4,[14] CdS[9]), and morphology control (e.g., nanoparticles,[15] hollow spheres,[16] nanosheets,[11] or flower-like[17] structures). In photocatalysis, the size and morphology of a material are crucial in determining the adsorption capabilities of the cata-

*Corresponding author's e-mail:
xiaotianli@jlu.edu.cn(X. Li)

lyst's surface towards target pollutants and the active sites that play a pivotal role during a photocatalytic process.[18—20] In gas sensing, the adsorption of oxygen on a material's surface is a key determinant of its gas sensing properties,[21] closely related to the surface morphology. Consequently, ZnO with varying morphologies exhibits substantial differences in gas sensing properties.[21–23]

In this study, we synthesize ZnO materials using a sol-gel-hydrothermal method in a binary solvent system of water and ethylene glycol, producing a variety of ZnO samples. By fine-tuning the zinc acetate concentration, we precisely control the morphology of the resulting ZnO structures. We investigate the fundamental structural characteristics, as well as the photocatalytic and gas-sensing properties of these samples. In photocatalysis, we evaluate the material's efficiency in the ultraviolet (UV) photocatalytic degradation of Rhodamine B (RB), identify the active radicals involved in photocatalysis, and evaluate the material's recyclability. For gas-sensing applications, we conduct a series of performance tests at various temperatures, gas concentrations, and cyclic conditions, measuring response and recovery times, and responses in different atmospheres. This detailed analysis enables a thorough comparison of the gas-sensing capabilities of our ZnO samples.

2 EXPERIMENT SECTION

2.1 Synthesis

ZnO was synthesized using a combined sol-gel and hydrothermal method. Specific amounts of zinc acetate and monoethanolamine were added to 20 mL of ethylene glycol, followed by magnetic stirring at 60 °C for 30 min. Then, 10 mL of deionized water was added, and the mixture was stirred for another hour. The resulting milky solution was transferred to a 50 mL Teflon-lined autoclave and heated at 180 °C for 10 h. The white precipitate was centrifuged, washed sequentially with water and alcohol, and dried at 60 °C for 10 h. The final ZnO product was obtained by annealing the dried material at 500 °C for 2 h. In this series, zinc acetate and monoethanolamine were added in amounts of 0.11 g and 30 μL, 0.15 g and 45 μL, and 0.3 g and 90 μL, respectively, with the corresponding samples labeled as ZnO-1, ZnO-2, and ZnO-3.

2.2 Characterization

Crystallographic structures were studied with a D8 Tools X-ray diffractometer with Cu Kα (λ = 0.15405 nm). The morphology and microstructure of the as-prepared samples were observed with a scanning electron microscope (SEM/EDS, JEOL JSM-6700F) and a transmission electron microscope (TEM, JEM 3010 and Tecnai G2 F20). UV/visible absorption spectrum was measured with a UV-2550 spectrophotometer. A fluorescence spectrophotometer (Perkin Elmer LS 55) was used to obtain the photoluminescence (PL) spectra. Photoelectrochemical measurements were performed using a computer-controlled workstation (CHI650D, Shanghai, Chenhua Co., China).

2.3 Photocatalytic reactions

The photocatalytic performance was assessed using Rhodamine B (RB) as the target organic pollutant, with a concentration of 10 mg·L^{-1} in a 100 mL solution. A total of 20 mg of the catalyst was introduced into the RB solution. Before initiating the photocatalytic reaction, the catalyst and RB solution were mixed and stirred in the dark for 30 min to ensure adsorption equilibrium. The photocatalytic reaction was then carried out under ultraviolet (UV) light irradiation. At 5 min intervals, 3 mL aliquots of the reaction mixture were collected, centrifuged, and the supernatant was analyzed. The RB concentration was measured using a UV-visible spectrophotometer.

2.4 Free radical capture experiment

Before the photocatalytic test, specific scavengers for active species were added. By comparing the pollutant degradation efficiency with and without these scavengers, the role of active species in the photocatalytic process was determined. Tert-butanol (t-BuOH), sodium ethylenediaminetetraacetate (EDTA), and benzoquinone (BQ) were used as scavengers for hydroxyl radicals (OH), holes (h^+), and superoxide radicals (O^{2-}), respectively, each at 1 mM·L^{-1}.

2.5 Gas sensing performance testing

Gas sensing performance was evaluated using the CGS-1TP intelligent gas sensing analysis system, produced by Beijing Elite Technology Co., Ltd. Prior to the test, 0.1 g of a ZnO sample was mixed and ground with alcohol in a mortar, then evenly applied to a ceramic sample plate. The sample was left to air-dry and naturally age for 24 h, after which it was used to fabricate a gas sensor device. For the test, the device was positioned on a temperature-controlled platform within a gas chamber, secured with probes, and connected to the testing electrodes. Measurements commenced once the resistance of the sample stabilized at the testing temperature.

The device's stable resistance in air was labeled as Ra, and in the presence of the target gas, as Rg. Sensitivity was calculated as the Ra/Rg ratio. The test atmosphere comprised five gases: ethanol, acetone, methanol, formaldehyde, and benzene.

3 RESULTS AND DISCUSSION

3.1 Characterization

Figure 1 shows XRD spectra of the samples. All diffraction peaks match the hexagonal wurtzite structure (JCPDS 36-1451). This confirms that all ZnO samples

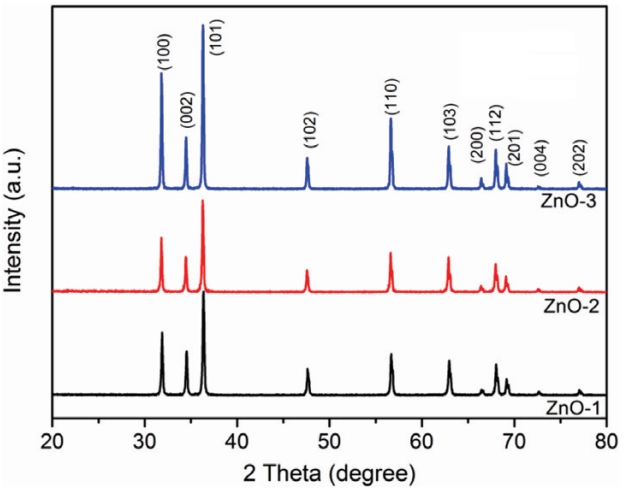

Figure 1: XRD patterns of the samples

have a hexagonal wurtzite structure and are well-crystallized. Moreover, the FWHM of the diffraction peaks decreases with increasing zinc acetate concentration, indicating higher crystallinity in the corresponding ZnO samples.

Figure 2 shows SEM images of the samples, revealing significant morphological changes with increasing zinc acetate concentration during synthesis. The ZnO-1 sample (**Figures 2a**, a-1) consists mainly of individual, dispersed porous granules with particle sizes ranging from 100–200 nm. Some granules have hexagonal edges, and a few double and triple particles are observed. The ZnO-2 sample (**Figures 2b**, b-1) has a granular shape similar to ZnO-1 but with a broader size range of 200–500 nm, indicating greater size variation and the presence of larger particles.

The ZnO-3 sample (**Figures 2c**, c-1) shows a distinctive grenade-like morphology, with lengths of 2–4 μm. This structure is formed by the union of two hexagonal prisms of differing sizes, characterized by flat cross-sections, rounded side edges, and a relatively smooth surface. The length distribution is uneven, akin to the morphology described in the literature.[8] This grenade-like shape is typical of wurtzite ZnO, signifying a stable crystal structure and a high degree of crystallinity.[11]

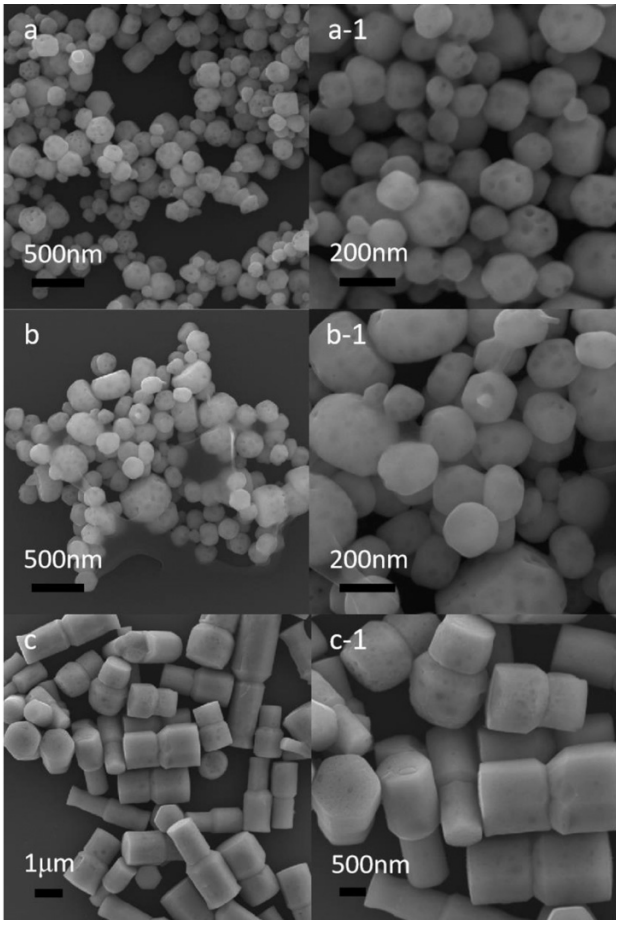

Figure 2: SEM images of ZnO-1 (a, a-1), ZnO-2 (b, b-1), and ZnO-3 (c, c-1)

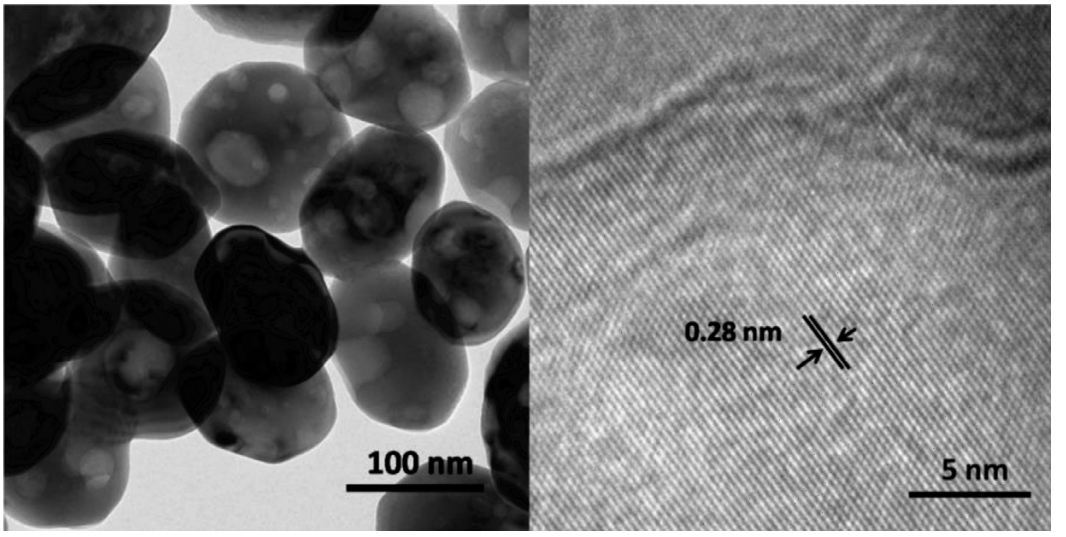

Figure 3: a) TEM and b) HRTEM images of ZnO-1

To further study the microstructures of the ZnO samples, TEM and HRTEM analyses were performed on ZnO-1. As shown in **Figure 3a**, the particle sizes range from 100 to 150 nm. The image also reveals larger, irregularly shaped pores, consistent with the SEM results. These pores have diameters of 10–50 nm. In the HRTEM image (**Figure 3b**), distinct lattice fringes are visible, with a spacing of approximately 0.28 nm, corresponding to the (100) plane of ZnO.

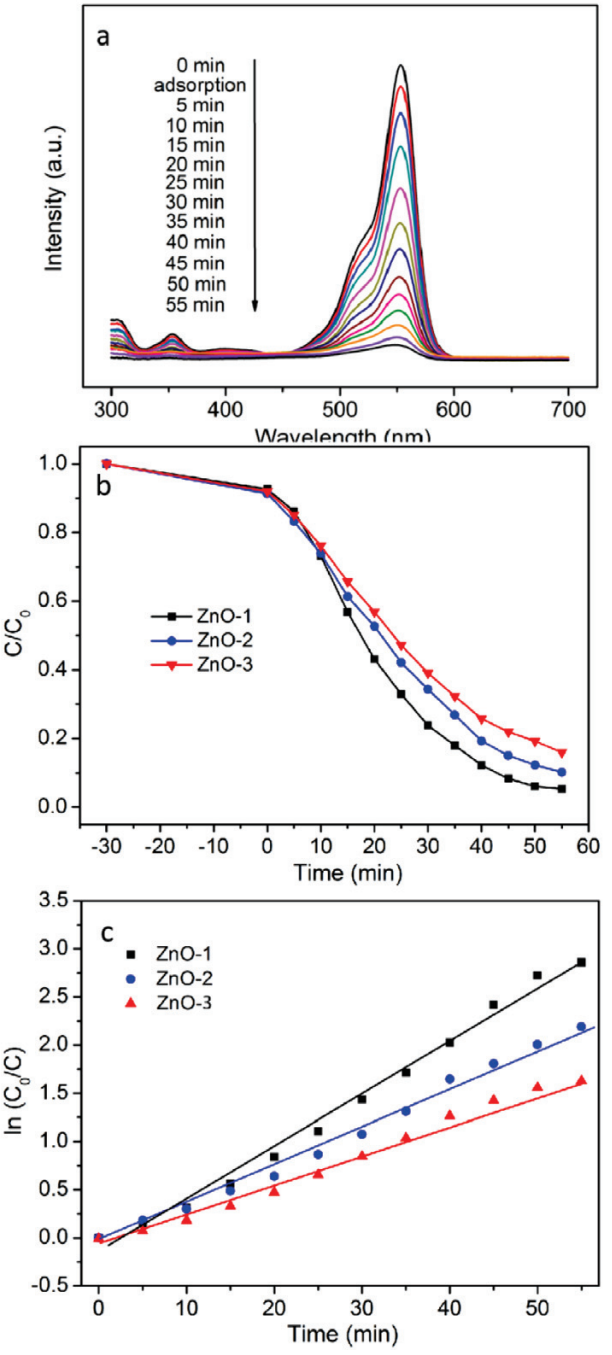

Figure 4: a) Absorption spectra of RB solution degraded by ZnO-1 under UV light; b) photocatalytic degradation of RB by ZnO series samples; c) the corresponding curves between ln(C/C_0) and degradation time

3.2 Photocatalytic behavior

We evaluated the photocatalytic performance of the ZnO series samples using the organic dye RB as the target pollutant, with results presented in **Figure 4**. **Figure 4a** shows the absorption spectrum of ZnO-1 during photocatalytic degradation of RB under UV light. The intensity of the characteristic absorption peak of RB near 550 nm gradually diminished upon UV exposure, indicating progressive degradation. After 55 min, RB is nearly fully degraded.

Figure 4b illustrates the changes in the RB concentration over time for the series samples, where C_0 represents the initial concentration and C is the real-time concentration. The photocatalytic efficiency decreased in the order ZnO-1 > ZnO-2 > ZnO-3, achieving RB degradation rates of (94.7, 89.8, and 84.0) % after 55 min, respectively. All photodegradations processes of RB were found to follow the Langmuir–Hinshelwood first-order kinetics model.[25] The model can be expressed by $\ln(C_0/C) = kt$, where k is the decomposition rate constant. The calculated k values for ZnO-1, ZnO-2, and ZnO-3 were (0.054, 0.039, and 0.029) min^{-1}, respectively. Combined with the SEM results, the ZnO-1 sample, which had the smallest particle size, exhibited the highest photocatalytic activity.

To investigate the stability of the samples, photocatalytic cycling tests were conducted on the ZnO-1 sample, with the results shown in **Figure 5**. After six rounds of photocatalytic experiments, the degradation efficiency remained at 88.5 %, indicating good chemical stability.

3.3 Photocatalytic mechanism

To elucidate the mechanism underlying the differences in photocatalytic performance among the ZnO series samples, we conducted photoluminescence (PL) tests, with the results shown in **Figure 6a**. Each sample exhibits a UV emission peak at approximately 395 nm, corresponding to the recombination luminescence of

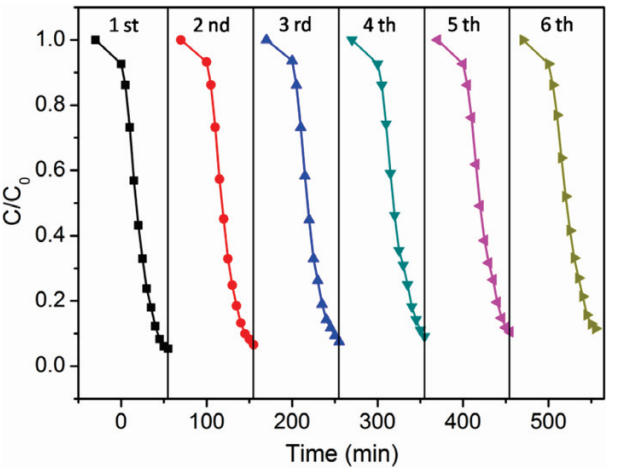

Figure 5: Photocatalytic reusability of ZnO-1

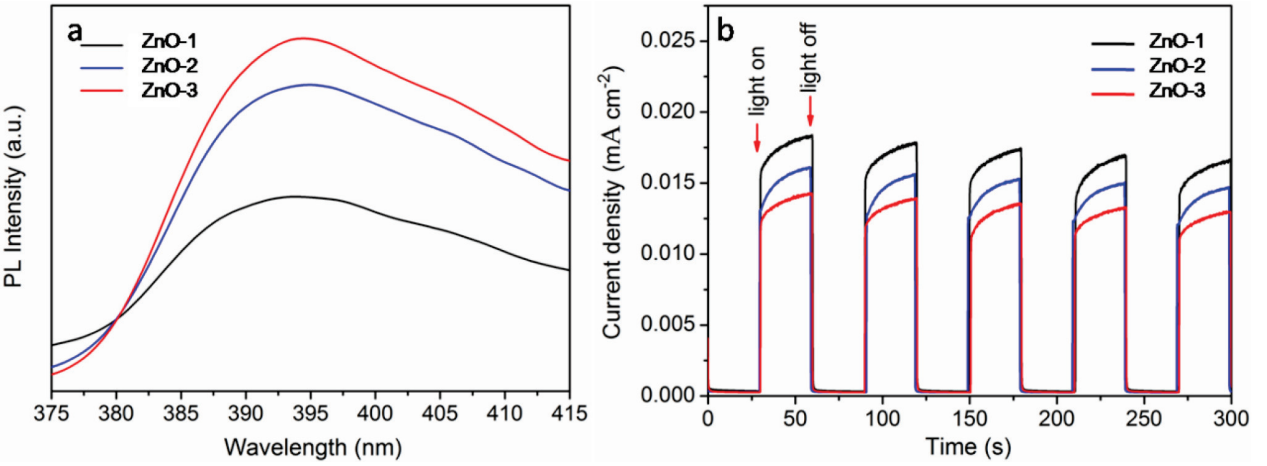

Figure 6: a) Photoluminescence (PL) spectra of samples; b) I-T (current-time) curves of samples under UV light

inter-band photogenerated electron-hole pairs in ZnO.[26] The intensity of this peak increased significantly from ZnO-1 to ZnO-3, indicating a pronounced enhancement in carrier recombination. According to the photocatalytic theory, an increased recombination rate of photogenerated electron-hole pairs reduces photocatalytic efficiency, leading to a sequential decline in performance from ZnO-1 to ZnO-3. Furthermore, by combining these findings with prior XRD and SEM data, we conclude that as the Zn^{2+} concentration increased during synthesis, ZnO crystals underwent rapid growth and size expansion. This growth likely elevated the concentration of lattice defects, which act as recombination centers for free excitons, thereby intensifying ZnO's intrinsic luminescence peak.

The photocurrent response of photocatalytic materials in an electrochemical environment serves as a reliable indicator for evaluating the generation, separation, and transfer of photogenerated electron-hole pairs during photocatalysis. A stronger photocurrent response indicates a more efficient separation of these pairs. **Figure 6b** shows the photocurrent test results for the ZnO samples. Upon illumination, the photocurrent increased rapidly and returned to its baseline promptly after the light was turned off, demonstrating excellent stability and repeatability of the response. The photocurrent intensities of the samples followed the following order: ZnO-1 > ZnO-2 > ZnO-3. This result confirms that ZnO-1, which has the smallest particle size, achieved the highest photogenerated charge carrier separation efficiency, consistent with the PL data. Consequently, ZnO-1 also exhibited the best photocatalytic performance in the degradation tests.

To ascertain the primary active radicals participating in the photocatalytic process and to delve into the underlying mechanism, we performed radical trapping experiments using ZnO-1 as the representative sample. The findings, presented in **Figure 7**, reveal that the inclusion of EDTA exerts a minimal influence on the photocatalytic process, indicating that h^+ is not a dominant factor in the reaction. Conversely, the addition of t-BuOH exerts a noticeable effect on the degradation efficiency of RB, suggesting the involvement of OH in the photocatalytic process. Most notably, the introduction of BQ substantially inhibits the photocatalytic degradation of RB, thereby establishing O^{2-} as the most significant active radical contributing to the photocatalytic process.

Based on the aforementioned analysis, the photocatalytic process involves the excitation of valence band electrons in the ZnO material by UV light, causing them to transition to the conduction band and leaving an equal number of holes in the valence band. The conduction band electrons then react with adsorbed oxygen on the material's surface, generating a significant amount of O^{2-} radicals. These radicals can further react with conduction band electrons and hydrogen ions in water to produce H_2O_2 and OH. Simultaneously, the valence band holes react with water ions, also producing OH radicals. These highly reactive species, with their strong oxidizing capabilities, ultimately lead to the complete degradation of the organic dye RB. The entire photocatalytic reaction process can be summarized as follows:

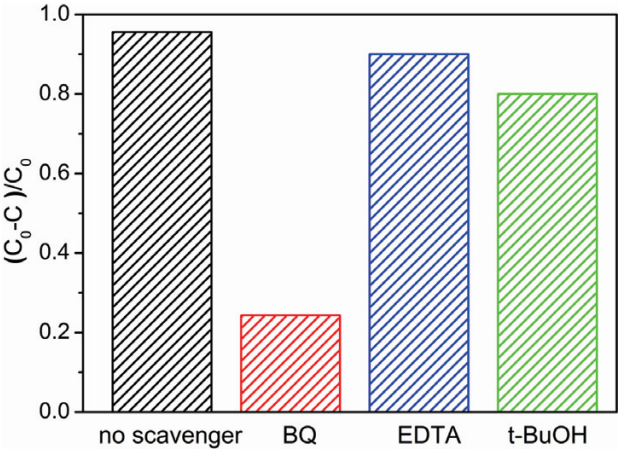

Figure 7: Effects of different scavengers on the photocatalytic efficiency of ZnO-1

Table 1: Responses of ZnO sensors to ethanol with different concentrations

Concentration/ppm	5	10	20	40	60	80	100	200
Response of ZnO-1	1.6	2.0	3.4	4.4	6.6	9.3	12.6	15.3
Response of ZnO-2	1.6	2.1	3.7	5.3	8.4	11.3	15.6	20.5
Response of ZnO-3	1.8	2.2	3.0	3.5	4.6	5.9	8.0	

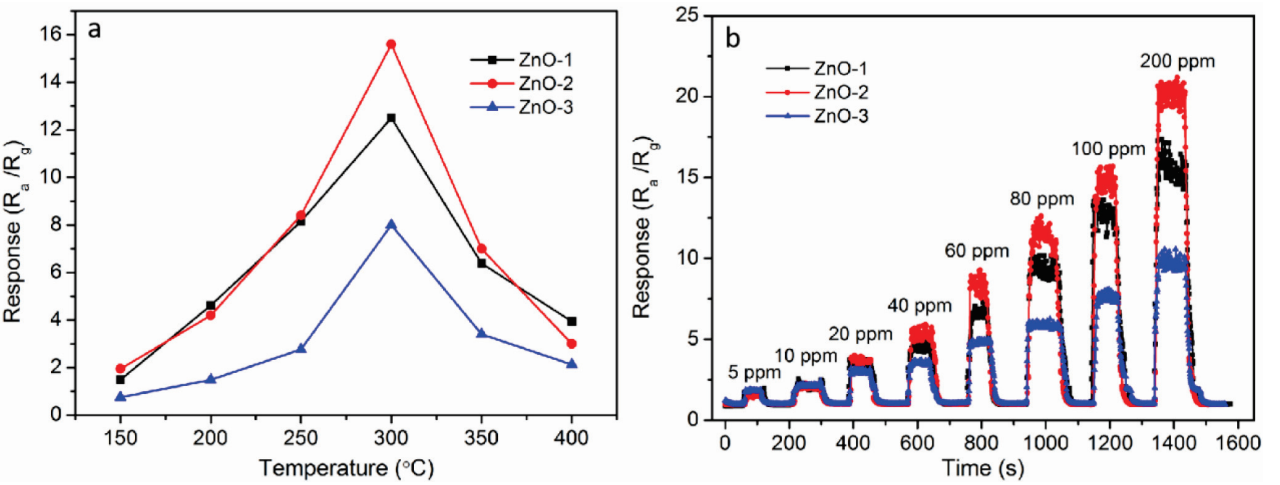

Figure 8: a) Response versus operating temperature of ZnO sensors upon exposure to 100 ppm ethanol; b) response-recovery curves of ZnO sensors to ethanol at different concentrations

$$ZnO + h\nu \rightarrow ZnO\ (h^+ + e^-) \quad (1)$$

$$e^- + O_2 \rightarrow O_2^- \quad (2)$$

$$O_2^- + e^- + 2H^+ \rightarrow H_2O_2 \quad (3)$$

$$H_2O_2 + e^- \rightarrow OH + OH^- \quad (4)$$

$$RB + O_2^-, OH, h^+ \rightarrow Products \quad (5)$$

3.4 Gas sensing properties

It is widely recognized that the gas-sensing performance of materials is intricately linked to their operating temperature. To determine the optimal operating temperature for our samples, we initially conducted tests on the ZnO series to assess their sensitivity to 100 ppm ethanol gas across a temperature range of 150–400 °C, as illustrated in **Figure 8a**. The response values of the three samples consistently displayed a pattern of the initial increase followed by a decrease as the temperature rose, each reaching its peak response at 300 °C. Consequently, all further gas-sensing performance evaluations were carried out at this identified optimal temperature. At this optimal operating temperature, the response values of the three samples, ZnO-3, ZnO-1, and ZnO-2, ranked from the lowest to the highest, were 8.0, 12.5, and 15.6. It is worth mentioning that these response values are significantly superior to those of our previous Ce:ZnO composites.[27]

Figure 8b shows response and recovery curves of the ZnO series samples exposed to various concentrations of ethanol gas. Upon the introduction of ethanol gas, the samples' response values increase rapidly. As the ethanol gas concentration rises from 5 ppm to 200 ppm, the sensitivity of all three samples gradually increases. Their specific values are presented in **Table 1**.

In accordance with the unified standard for the detection limit of gas-sensing materials, which requires a response value greater than 3,[24,28] the detection limit for ZnO-1 and ZnO-2 samples is approximately 20 ppm, whereas for ZnO-3, it is around 40 ppm. Beyond 40 ppm, the disparity in response values among the three samples increases progressively, with ZnO-1 and ZnO-2 demonstrating enhanced sensitivity to gas concentration changes and consequently exhibiting correspondingly higher responses.

Selectivity is a crucial factor in assessing the overall performance of gas-sensing devices. **Figure 9** provides a comparison of the sensitivity of ZnO series samples to various gases at a concentration of 100 ppm, including

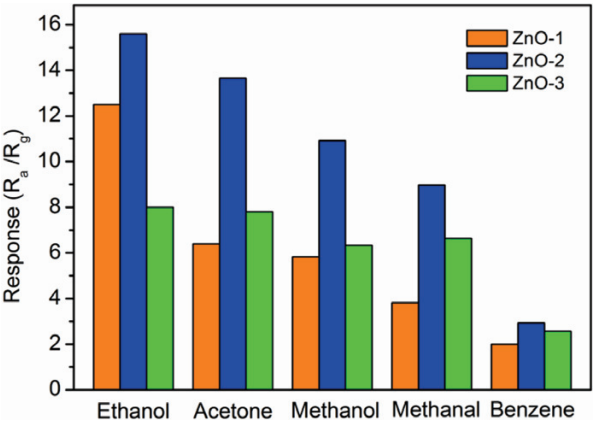

Figure 9: Responses of ZnO sensors to different gases (100 ppm)

ethanol, acetone, methanol, formaldehyde, and benzene. The data clearly illustrate that the ZnO-2 sample exhibits superior sensitivity across all tested gases compared to the other two samples, with its highest sensitivity particularly notable for ethanol. Nonetheless, the minimal difference in its sensitivity to acetone and methanol suggests limited selectivity. Among the samples, ZnO-3 exhibits the poorest selectivity, whereas ZnO-1 stands out with the best selectivity, demonstrating a significantly higher sensitivity to ethanol compared to other gases.

Figure 10a illustrates the four response and recovery cycles of the three ZnO sensors exposed to 100 ppm ethanol. Upon the introduction of ethanol gas, the sensitivity of all three samples promptly rises, and upon reverting to an air atmosphere, it swiftly returns to its initial values. The sensitivity, along with the response and recovery times, remains consistently stable throughout the four repeated tests, demonstrating the excellent reproducibility of the samples for ethanol detection.

To ascertain the response and recovery times of the samples, **Figure 10b** presents the single response and recovery curve of the ZnO-2 sample exposed to 100 ppm ethanol. In accordance with the widely accepted definitions of response time,[11,16] the response time is defined as the duration required for the device resistance to transition from its initial value to 90 % of the stable resistance value upon contact with the target gas. Conversely, the recovery time is defined as the period it takes for the device resistance to revert to 10 % of the stable resistance value after being removed from the target gas atmosphere. As illustrated in the figure, the sample demonstrates an exceptionally rapid instantaneous response and recovery, with respective times of 6 s and 25 s, which is shorter than the data reported in the literature for sensors based on ZnO[29] and ZnO composites (ZnO/Al_2O_3).[30] The response and recovery times of the other two samples under identical conditions are comparable to those of the ZnO-2 sample.

Based on the above comprehensive analysis, the optimal operating temperature for the ZnO series samples is approximately 300 °C, at which they demonstrate rapid response and recovery rates, along with excellent cyclic stability. At this temperature, samples ZnO-1 and ZnO-2 exhibit higher response to 100 ppm ethanol, with ZnO-1 particularly showcasing the best selectivity towards ethanol. SEM and TEM results reveal that samples ZnO-1 and ZnO-2 have a porous particulate morphology, whereas sample ZnO-3 features a grenade-like structure. Among the ZnO series samples exhibiting these two distinct morphologies, those with a smaller size and porous particulate morphology deliver superior gas-sensing performance, underscoring the profound influence of morphological differences on the gas-sensing properties of the samples.

3.5 Gas sensing mechanism

Typically, the sensitivity of gas-sensing materials is determined by the ratio of the sensor resistance in air to that in an ethanol atmosphere, known as Ra/Rg. When ZnO samples of various morphologies are exposed to an air atmosphere, the oxygen present adsorbs onto the ZnO surface, capturing electrons from the conduction band of the sample, thereby generating corresponding negative ion groups, such as O_2^-, O^-, and O^{2-}. The reactions are represented with the following equations:[31—34]

$$O_{2(air)} \rightarrow O_{2(ads)} \quad (6)$$

$$O_{2(ads)} + e^- \rightarrow O_{2(ads)}^- \quad (7)$$

$$O_{2(ads)}^- + e^- \rightarrow 2O_{(ads)}^- \quad (8)$$

$$O_{(ads)}^- + e^- \rightarrow O_{(ads)}^{2-} \quad (9)$$

Among these, $O_{2(air)}$ signifies the oxygen present in the air, whereas $O_{2(ads)}$ refers to the oxygen adsorbed onto the ZnO sensor surface. These reaction processes lead to

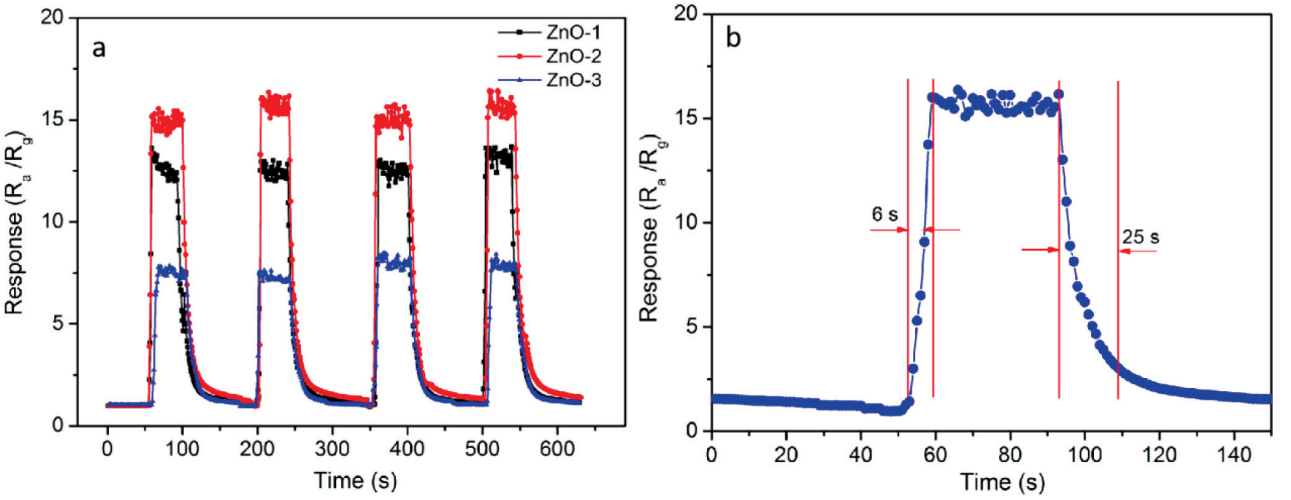

Figure 10: a) Response and recovery repeatability curves relating to 100 ppm ethanol for the sensors; b) single-cycle response and recovery curve of ZnO-2

a decrease in the electron concentration within ZnO, thereby forming an electron depletion layer of a specific thickness on the surface. This, in turn, results in an increase in the device resistance, denoted as Ra. When the sample is exposed to the target gas atmosphere, such as ethanol, the ethanol gas quickly adsorbs onto the surface of the ZnO sample and reacts with the surface oxygen ion groups. The reaction equations are as follows:[35,36]

$$C_2H_5OH_{(air)} \rightarrow C_2H_5OH_{(ads)} \quad (10)$$

$$C_2H_5OH_{(ads)} + 6O_{(ads)}^{-} \rightarrow 2CO_2 + 3H_2O + 6e^- \quad (11)$$

$$C_2H_5OH_{(ads)} + 6O_{(ads)}^{2-} \rightarrow 2CO_2 + 3H_2O + 12e^- \quad (12)$$

$$C_2H_5OH_{(ads)} + 3O_{2(ads)}^{-} \rightarrow 2CO_2 + 3H_2O + 3e^- \quad (13)$$

In this context, $C_2H_5OH_{(air)}$ signifies ethanol molecules present in the air, whereas $C_2H_5OH_{(ads)}$ refers to those ethanol molecules that have been adsorbed onto the surface of ZnO. The interaction between these adsorbed ethanol molecules and the oxygen ion groups on the sample surface prompts the release of trapped electrons back into the conduction band of ZnO. This process leads to a reduction in the thickness of the electron depletion layer and a swift decline in the resistance Rg.[12]

It is evident that a larger Ra/Rg value corresponds to a higher gas-sensing response in the material. The resistance values across different atmospheres are influenced by the thickness of the electron depletion layer, formed due to oxygen adsorption on the surface of a gas-sensing material – a phenomenon closely tied to the material's surface morphology. Samples characterized by a larger specific surface area and smaller size exhibit a stronger capacity for oxygen adsorption, typically resulting in a higher Ra value in air and, consequently, a more pronounced gas-sensitivity response.

SEM and TEM analyses reveal that within the series of ZnO samples we prepared, ZnO-3 and ZnO-4, due to their larger particle size, are minimally affected by the surface-adsorbed oxygen in terms of internal electron dynamics, leading to a smaller Ra value. Conversely, ZnO-1 and ZnO-2 exhibit similar porous morphologies, with larger pores distributed both externally and internally. This structure enhances gas diffusion and reaction kinetics by providing more channels and space within the material. Additionally, the increased number of electrons in the electron depletion layer results in a larger Ra value, thereby giving these two samples enhanced gas-sensing performance.

4 CONCLUSIONS

In a binary solvent system comprising water and ethylene glycol, we successfully synthesized a series of ZnO samples through a sol-gel-hydrothermal method. Our research revealed that by precisely controlling the concentration of the zinc source, we could tailor the morphology of the samples, thereby producing two distinct types of particulate morphologies: porous particles and grenade-like structures. Notably, as the particle size increased, the photocatalytic performance gradually decreased. Among them, the ZnO-1 sample, characterized by its smallest particle size, exhibited the highest photocatalytic rate of 0.054 min^{-1}. Radical scavenging experiments further indicated that superoxide anion (O^{2-}) was the most significant active radical contributing to the photocatalytic process. In terms of gas-sensing performance, our tests identified an optimal working temperature of around 300 °C for detecting ethanol vapor, with the ZnO-1 and ZnO-2 samples showing particularly high response values of 12.5 and 15.6, respectively. All samples demonstrated excellent cyclic stability and response/recovery times. Selectivity tests involving five different vapors – ethanol, acetone, methanol, formaldehyde, and benzene – highlighted the superior selectivity of the ZnO-1 sample towards ethanol. This enhanced selectivity is attributed to the unique combination of its small size and porous morphology, which enhance gas diffusion and surface interactions.

Building upon this work, future research will further explore the applications of ZnO porous materials in photocatalysis and gas sensors. This includes enhancing visible-light-responsive photocatalytic performance through structural design and elemental doping, as well as developing gas sensors with visible-light-response capabilities.

Acknowledgements

This work was supported by the Natural Science Foundation of Jilin Province (No. 20210101407JC).

5 REFERENCES

[1] W. L. Ong, S. Naarajan, B. Kloostra, Metal nanoparticle-loaded hierarchically assembled ZnO nanoflakes for enhanced photocatalytic performance, Nanoscale, 5 (**2013**), 5568–5575

[2] S. T. Kochuveedu, Y. H. Jang, D. H. Kim, A study on the mechanism for the interaction of light with noble metal-metal oxide semiconductor nanostructures for various photophysical applications, Chem. Soc. Rev., 42 (**2013**), 8467–8493

[3] A. A. Shaikh, M. R. Patil, B. S. Jagdale, V. A. Adole, Synthesis and characterization of Ag doped ZnO nanomaterial as an effective photocatalyst for photocatalytic degradation of Eriochrome Black T dye and antimicrobial agent, Inorg. Chem. Commun., 151 (**2023**), 110570

[4] L. Sun, D. Zhao, Z. Song, C. Shan, Z. Zhang, B. Li, D. Shen, Gold nanoparticles modified ZnO nanorods with improved photocatalytic activity, J. Colloid Interface Sci., 363 (**2011**), 175–181

[5] M. R. Hoffmann, S. T. Martin, W. Choi, D. W. Bahnemann, Environmental applications of semiconductor photocatalysis, Chem. Rev., 95 (**1995**), 69–96

[6] N. Serpone, A. V. Emeline, Semiconductor photocatalysis: past, present, and future outlook, J. Phys. Chem. Lett., 3 (**2012**), 673–677

[7] S. Senapati, S. K. Srivastava, S. B. Singh, Synthesis, characterization and photocatalytic activity of magnetically separable hexagonal Ni/ZnO nanostructure, Nanoscale, 4 (**2012**), 6604–6612

[8] T. Wang, S. S. Xu, N. T. Hu, H. Jun, J. Da, Microwave preparation and remarkable ethanol sensing properties of ZnO particles with con-

trolled morphologies in water-ethylene glycol binary solvent system, Sensors and Actuators B: Chemical, 255 (**2018**), 1006–1014

[9] X. Geng, J. J. You, C. Zhang, Microstructure and sensing properties of CdS-ZnO_{1-x} coatings deposited by liquid plasma spray and treated with hydrogen peroxide solution for nitrogen dioxide detection at room temperature, Journal of Alloys and Compounds, 687 (**2016**), 286–293

[10] F. Y. Fan, J. J. Zhang, J. Li, N. Zhang, R. R. Hong, X. C. Deng, P. G. Tang, D. Q. Li, Hydrogen sensing properties of Pt-Au bimetallic nanoparticles loaded on ZnO nanorods, Sensors and Actuators B: Chemical, 241 (**2017**), 895–903

[11] X. X. Xing, T. Chen, R. J. Zhao, Z. Z. Wang, Y. D. Wang, A low temperature butane gas sensor used Pt nanoparticles-modified AZO macro/mesoporous nanosheets as sensing material, Sensors and Actuators B: Chemical, 254 (**2018**), 227–238

[12] H. Chen, S. Y. Ma, H. Y. Jiao, G. J. Yang, X. L. Xu, T. T. Wang, X. H. Jiang, Z. Y. Zhang, The effect microstructure on the gas properties of Ag doped zinc oxide sensors: Spheres and sea-urchin-like nanostructures, J. Alloys Compd., 687 (**2016**), 342–351

[13] X. LIu, Y. Sun, M. Yu, Y. Yin, B. Du, W. Tang, T. Jiang, B. Yang, W. Cao, Enhanced ethanol sensing properties of ultrathin ZnO nanosheets decorated with CuO nanoparticles, Sensors and Actuators B: Chemical, 255 (**2018**), 3384–3390

[14] D. Kim, K. Yong, Boron doping induced charge transfer switching of a C_3N_4/ZnO photocatalyst from Z-scheme to type II to enhance photocatalytic hydrogen production, Appl. Catal. B, 282 (**2021**), 119538

[15] L. V. Vijayan, J. P. A. Jose, Stability Studies of Cohesive Soil with Nano Magnesium and Zinc Oxide, Materials and Technology, 56 (**2022**) 2, 187–191

[16] B. Q. Han, X. Liu, X. X. Xing, N. Chen, X. C. Xiao, S. Y. Liu, Y. D. Wang, A high response butanol gas sensor based on ZnO hollow spheres, Sensors and Actuators B: Chemical, 237 (**2016**), 423–430

[17] T. F. Bi, Z. X. Du, S. Y. Chen, H. He, X. M. Shen, Y. C. Fu, Preparation of flower-like ZnO photocatalyst with oxygen vacancy to enhance the photocatalytic degradation of methyl orange, Appl. Surf. Sci., 614 (**2023**), 156240

[18] S. K. Wu, X. P. Shen, G. X. Zhu, H. Zhou, Z. Y. Ji, K. M. Chen, A. H. Yuan, Synthesis of ternary Ag/ZnO/$ZnFe_2O_4$ porous and hollow nanostructures with enhanced photocatalytic activity, Appl. Catal. B, 184 (**2016**), 328–336

[19] R. Gupt, N. K. R. Eswar, J. M. Modak, G. Madras, Effect of morphology of zinc oxide in ZnO-CdS-Ag ternary nanocomposite towards photocatalytic inactivation of E. coli under UV and visible light, Chem. Eng. J., 307 (**2017**), 966–980

[20] F. P. Peng, Q. Zhou, C. H. Lu, Y. R. Ni, J. H. Kou, Z. Z. Xu, Construction of (001) facets exposed ZnO nanosheets on magnetically driven cilia film for highly active photocatalysis, Appl. Surf. Sci., 394 (**2017**), 115–124

[21] C. Li, C. Feng, F. Qu, J. Liu, L. Zhu, Y. Lin, Y. Wang, F. Li, J. Zhou, S. Ruan, Electrospun nanofibers of p-type NiO/n-type ZnO heterojunction with different NiO content and its influence on trimethylamine sensing properties, Sensors and Actuators B: Chemical, 207 (**2015**), 90–96

[22] M. Akermi, N. Sakly, R. B. Chaabane, H. B. Ouada, Effect of PEG-400 on the morphology and electrical properties of ZnO nanoparticles application for gas sensor, Mater. Sci. Semicond. Process., 16 (**2013**) 3, 807–817

[23] R. Ferro, The effect of the material morphology on the response of the NO_2 sensor based on ZnO thin film, Sensors and Actuators B: Chemical, 143 (**2009**) 1, 99–102

[24] J. Y. Liu, T. S. Wang, B. Q. Wang, P. Sun, Q. Y. Yang, G. Y. Lu, Highly sensitive and low detection limit of ethanol gas sensor based on hollow ZnO/SnO_2 spheres composite material, Sensors and Actuators B: Chemical, 245 (**2017**), 551–559

[25] K. Vasanthkumar, K. Porkodi, F. Rocha, Langmuir–Hinshelwood kinetics – A theoretical study, Catal. Commun., 9 (**2008**) 1, 82–84

[26] L. Wang, Z. Y. Ji, J. J. Lin, P. Li, Preparation and optical and photocatalytic properties of Ce-doped ZnO microstructures by simple solution method, Mater. Sci. Semicond. Process., 71 (**2017**), 401–408

[27] H. X. Chen, H Yu, S. Cui, J. H. Xu, Y. Zhang, C. Y. Liu, Synthesis of Ce:ZnO nanocomposites: Facile synthesis and fast acetone gas sensing response properties, Physica B, 516 (**2017**), 36–40

[28] L. Shi, J. Cui, F. Zhao, D. Wang, Y. Lin, High-performance formaldehyde gas-sensors based on three dimensional center-hollow ZnO, Phys. Chem. Chem. Phys., 17 (**2015**), 31316–31323

[29] N. F. Hamedani, A. R. Mahjoub, A. A. Khodadadi, Y. Mortazavi, CeO_2 doped ZnO flower-like nanostructure sensor selective to ethanol in presence of CO and CH_4, Sens. Actuators B, 169 (**2012**), 67–73

[30] Q. H. Xu, D. M. Xu, M. Y. Guan, Y. Guo, Q. Qi, G. D. Li, ZnO/Al_2O_3/CeO_2 composite with enhanced gas sensing performance, Sens. Actuators B, 177 (**2013**), 1134–1141

[31] Y. Tian, J. C. Li, H. Xiong, J. N. Dai, Controlled synthesis of ZnO hollow microspheres via precursor-template method and its gas sensing property, Appl. Surf. Sci., 258 (**2012**), 8431–8438

[32] S. H. Yan, S. Y. Ma, W. Q. Li, X. L. Xu, L. Cheng, H. S. Song, X. Y. Liang, Synthesis of SnO_2-ZnO heterostructured nanofibers for enhanced ethanol gas-sensing performance, Sensors and Actuators B: Chemical, 221 (**2015**), 88–95

[33] L. Zhu, W. Zeng, Room-temperature gas sensing of ZnO-based gas sensor: A review, Sensors and Actuators A: Physical, 267 (**2017**), 242–261

[34] R. J. Zhao, K. J. Li, Z. Z. Wang, X. X. Xing, Y. D. Wang, Gas-sensing performances of Cd-doped ZnO nanoparticles synthesized by a surfactant-mediated method for n-butanol gas, J. Phys. Chem. Solids, 112 (**2018**), 43–49

[35] M. L. YIn, M. D. Liu, S. Z. Liu, Diameter regulated ZnO nanorod synthesis and its application in gas sensor optimization, J. Alloys Compd., 586 (**2014**), 436–440

[36] X. L. Deng, L. L. Zhang, J. Guo, Q. J. Chen, J. M. Ma, ZnO enhanced NiO-based gas sensors towards ethanol, Mater. Res. Bull., 90 (**2017**), 170–174